The Combined Method of Ray Tracing and Diffraction and Its Application to Ultra-wideband Pulse Propagation

Bingquan Chen[1] · **Chang Chen[1]** · **Hongyang Ma[1]**

Abstract

In this study the scattered-filed computation using the combined method of ray tracing and diffraction (CMRD) is revisited but with an extension to the backscattering computation. The concept of the equivalent phase object is considered as the key part in the developed CMRD method, and is analyzed mathematically with accurately derived expressions for its amplitude and phase function. A formulated CMRD method for the backscattering computation is developed in this work, which is then used in the forward modeling and numerical computations for ultra-wideband pulse propagation and backscattering from a perfectly conducting circular cylinder. The numerical simulation indicates that reasonable and good agreements can be achieved for comparisons between our CMRD method and exact eigenfunction expansion approach. It is expected that the theoretical model and method of backscattering calculation using CMRD can be applied to the image processing and target identification with measurements of backward-scattered electromagnetic and acoustic waves.

Keywords Phase object · Ray tracing · Diffraction · Backscattering · Electromagnetic propagation

1 Introduction

The development of theoretical method and algorithm for computing backscattering of time-harmonic electromagnetic or acoustic waves by objects of simple as well as nonsimple shapes is still a challenging issue in the field of imaging and target identification using backscattering measurements and related areas, which has attracted a lot of attention in the past because of its importance in a variety of different applications [1–5]. Even the exact solution of the scattered field by a simple shape such as a sphere or a cylinder can be expressed as an eigenfunction expansion [6], using such expansions in practice is often limited due to difficulties with the computation of the eigenfunctions. Thus, there have been some approaches with approximate methods and models for backscattering computation. Ruppin used the extended boundary condition for calculating the scattered field by a finite dielectric cylinder for a plane electromagnetic wave [1]. Zhu and Bjorno [3] developed a

✉ Bingquan Chen
chen_bingquan@yeah.net

[1] School of Sciences, Qingdao University of Technology, Qingdao 266033, China

parabolic equation model for computing backscattering in a cylindrical coordinate system. In the work of Jech et al. [4] the authors presented comparisons among the exact analytical models, approximate analytical models, and numerical models for computing acoustic backscattering by simple shapes. Mitri's [7] method used the partial-wave series solution for the linear scattering by an infinite circular cylinder. Follett et al. [8] used finite element method for backscattering computation of sound by a solid aluminium cylinder, which was compared with experimental data in their study.

The scattered-filed computation using the combined method of ray tracing and diffraction (CMRD) was formulated and discussed a numbers of years ago by one of the authors (BC) and a co-author in a paper published in *Applied Optics* [9]. In the study presented in this paper, the scattered-filed computation using CMRD is revisited but with an extension to the backscattering computation and a more applied view. This paper will mainly contain two parts: (1) We first present the theoretical analyses and discussions of the formulated CMRD method for the backscattering computation. (2) We then apply the CMRD method in the forward modeling and numerical computations for ultra-wideband (UWB) pulse propagation and backscattering from a perfectly conducting circular cylinder. The theoretical model and algorithm developed in this work might be important and useful for computations related to UWB propagation, imaging, and target identification problems.

In the field of electromagnetic (EM) wave propagation and imaging, there has been a need for investigating an accurate and efficient method for backscattering computation. In our study, we will our method with the "exact-solution" approach (i.e. the eigenfunction-expansion method), which indicates that our method is efficient and reasonably accurate. Our method and model have not been reported and addressed in any previous publications by other researchers in the field of backscattering computation associated with EM wave propagation, imaging, and target identification, and related applications.

2 CMRD-Based Theory for Backscattering Computation

In this section we present the detailed theoretical analyses and formulations for the backscattering computation using the combined method of ray tracing and diffraction. For simplicity, our attention in this paper will mainly focus on the two-dimensional (2-D) problem associated with backscattering by circular cylinders, including the formulated discussions in this section and the designed numerical simulations of backscattering from a perfectly conducting circular cylinder in next section. Note that the resulted model and formulations can be extended for solving the three-dimensional problems.

2.1 CMRD Theory of 2-D Problem

For a 2-D problem, we assume that a plane or cylindrical scalar wave field u^i, generated by the source S, is normally incident on a scatterer with axis normal to the x–z plane as shown in Fig. 1. The refractive indices of the scatterer and the surrounding medium are $n_2 = n'_2 + in''_2$ and n_1, respectively. n_2 is usually a complex number, and n''_2 represents the absorption. Let the z axis of the coordinate system pass through the source and the scatterer, and the total backward-scattered field is observed at $P(x, z)$.

Note that the concept of the equivalent phase object (EPO) [9] plays a key role in the CMRD method for backscattering computation. CMRD basically consists of two steps. In the first step, we replace the scatterer by an EPO, situated in the plane $z = b$ and occupying an
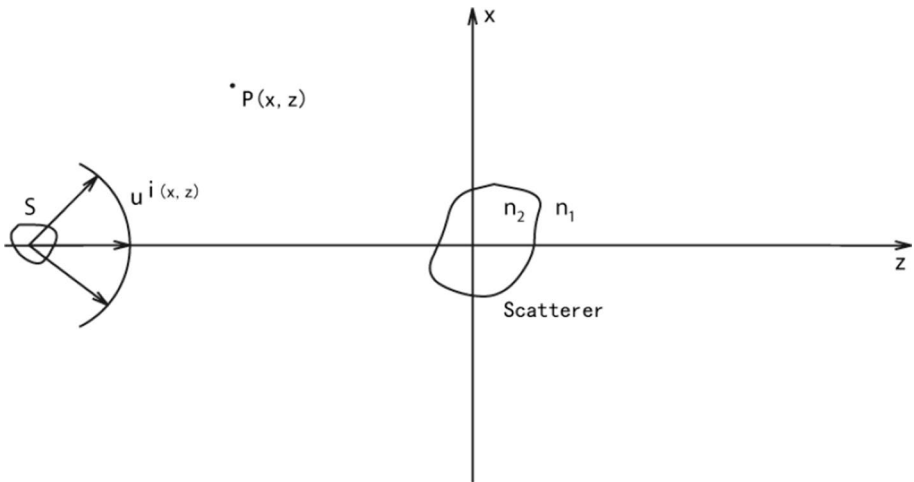
Fig. 1 2-D backscattering geometry

area $\mathcal{A}$. We then use ray tracing to determine the distance b and the area $\mathcal{A}$ of the EPO, as well as the amplitude function $a(x')$ and phase function $\phi(x')$ of the field at the EPO. Note that x' is the the variable of integration. The general procedure of ray tracing depends on the absolute value of the refractive-index difference $|n_2 - n_1|$, and on the size of the imaginary part of the refractive index n_2 of the scatterer. The approximate result of the propagating field in the plane $z = b$ can be obtained using ray tracing and the Kirchhoff approximation

$$u^B(x', b) = \begin{cases} 0 & \text{for } x' \notin \mathcal{A} \\ u^i(x', z = b)a(x')e^{i\phi(x')} & \text{for } x' \in \mathcal{A} \end{cases}, \tag{1}$$

where $u^i(x', b)$ is the incident field in the plane at $z = b$, and the amplitude function $a(x')$ and phase function $\phi(x')$ are to be determined from ray tracing. The superscript B of $u^B(x', b)$ in Eq. (1) is used to denote the *backward* propagating field component in the plane $z = b$, i.e. the field component propagating into the half-space $z < b$. Knowing the backward propagating field component in the plane $z = b$, we can use Rayleigh-Sommerfeld's first diffraction formula to obtain the field at the observation point $P(x, z)$ in the half-space $z < b$. Thus we have

$$u(x, z) = \int_{\mathcal{A}} u^B(x', b)h(x - x', z - b)dx', \tag{2}$$

where $u^B(x', b)$ is given in Eq. (1), and the impulse response $h(x - x', z - b)$ is given by

$$h(x - x', z - b) = 2\frac{\partial}{\partial z}G(x - x', z - b), \tag{3}$$

where $G(x - x', z - b)$ is the Green's function for 2-D wave propagation in the homogeneous medium of refractive index n_1 surrounding the scatterer. Thus we have

$$G(x - x', z - b) = -\frac{i}{4}H_0^{(1)}(k_1 R), \tag{4}$$

where $H_0^{(1)}(k_1 R)$ is the zeroth-order Hankel function of the first kind, and R is the distance from an integration point $(x', z = b)$ to the observation point $P(x, z)$, i.e.

$$R = \sqrt{(x - x')^2 + (z - b)^2}. \tag{5}$$

Thus, the backward-scattered field at observation point $P(x, z)$ is given by

$$u^{BS}(x, z) = \int_{\mathcal{A}} u^i(x', b) a(x') e^{i\phi(x')} h(x - x', z - b) dx'. \tag{6}$$

Carrying out the differentiation in Eq. (3) and assuming that $k_1 R \gg 1$ so that we can replace the Hankel function by its lowest-order asymptotic expansion, we obtain for the impulse response [10]

$$h(x - x', z - b) = \frac{1}{\sqrt{i\lambda_1}} \frac{z}{R^{3/2}} e^{ik_1 R}. \tag{7}$$

For the special case in which the incident field is a plane wave, we have

$$u^i(x', b) = e^{ik_1(s_x^i x' + s_z^i b)}, \tag{8}$$

so that Eq. (6) becomes

$$u^{BS}(x, z) = \frac{1}{\sqrt{i\lambda_1}} \int_{\mathcal{A}} a(x') e^{i\phi(x')} \frac{z}{R^{3/2}} e^{ik_1(R + s_x^i x' + s_z^i b)} dx'. \tag{9}$$

Note that the integrals in Eq. (9) can be computed accurately and efficiently using the Stamnes–Spjelkavik–Pedersen method for single integrals [10, 11].

2.2 EPOs for a Plane Wave Incident on a Circular Cylinder

As we mentioned above, the scatterer in Fig. 1 is now assumed to be a circular cylinder. Generally speaking, the backward-scattered field from the cylinder mainly contains the contributions from the following two parts: (1) The first equivalent phase object (EPO-1) represents that the wave is directly reflected backward at the interface between the surrounding medium and the cylinder. (2) The second equivalent phase object (EPO-2) represents that the wave is first refracted into the cylinder, then reflected at the other side of the cylinder, and finally refracted out of the cylinder in the backward direction. Note that for a ray that is reflected more than one time inside the cylinder and refracted out of the cylinder in the backward direction, its contribution is much less than that of EPO-1 and EPO-2 and will not be considered for backscattering computation. For both EPO-1 and EPO-2, we need to use ray tracing to determine the EOP position b and the size parameter w, as well as the amplitude function $a(x')$, and the phase function $\phi(x')$ of the field at each EPO. The subscripts 1 and 2 used in b, w, $a(x')$, and $\phi(x')$ below stand for EPO-1 and EPO-2, respectively.

2.2.1 EPO-1

Consider a plane wave normally incident on a circular cylinder with a radius of a. As show in Fig. 2, when a ray incident upon the cylinder at $\alpha = \pm \frac{\pi}{4}$, the direction of the reflected ray

Fig. 2 Geometry of EPO-1
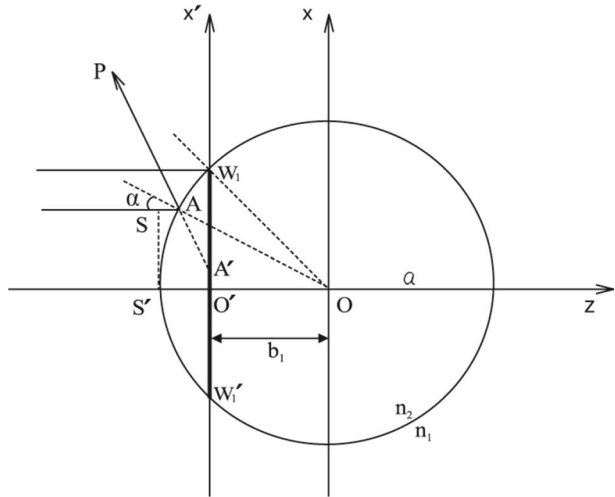
will be parallel to the vertical axis. Therefore, for the rays with angle of incidence in the range $[-\frac{\pi}{4}, +\frac{\pi}{4}]$ will be reflected in the backward direction, which is the physical origin of EPO-1. In Fig. 1, the EPO-1 (i.e. the line $W_1 W_1'$) is situated at $x = b_1$ and is of the width $2w_1$ along the x'-axis. The position parameter b_1 and half width w_1 are given by

$$b_1 = -a\cos\left(\frac{\pi}{4}\right), \quad w_1 = a\sin\left(\frac{\pi}{4}\right),$$

where a is the radius of the cylinder. Consider now ray SA, we extend the reflected ray backward until it intersects EPO-1 at point $A'(x', 0)$. Then for an incident ray of height $x = a\sin\alpha$ (i.e. the coordinate of A), the coordinate x' of A' can be obtained using geometrical relations

$$x'(\alpha) = a\left(\sin\alpha + \frac{1}{\sqrt{2}}\tan(2\alpha) - \cos\alpha\tan(2\alpha)\right), \tag{10}$$

where α is the angle of incidence as indicated in Fig. 2.

The phase $f_1(x')$ of reflected ray AA' at $A'(x', 0)$ is determined by

$$f_1(x') = kn_1(SA - AA'), \tag{11}$$

with

$$SA = a(1 - \cos\alpha),$$

$$AA' = \frac{a(\cos\alpha - 1/\sqrt{2})}{\cos 2\alpha}.$$

The phase $\phi_1(x')$ of EPO-1 should satisfy the following two conditions: (1) $\phi_1(x') = 0$ at the edge of EPO-1 for all values of refractive indices n_1 and n_2. (2) $\phi_1(x') = 0$ when $n_1 = n_2$. Thus, $\phi_1(x')$ can be expressed as

$$\phi_1(x') = f_1(x') - kn_1(a - |b_1|)$$

$$= -kn_1 a \frac{(\cos\alpha - 1/\sqrt{2})(\cos 2\alpha + 1)}{\cos 2\alpha}. \tag{12}$$

The amplitude $a_1(x')$ at EPO-1 can be given by

$$a_1(x') = a_1^0(x')|R_1(x')|, \tag{13}$$

where $R_1(x')$ is the Fresnel reflection coefficient, and

$$a_1^0(x') = \left|\frac{dx}{dx'}\right| = \left|\frac{a\cos\alpha}{dx'(\alpha)/d\alpha}\right|. \tag{14}$$

2.2.2 EPO-2

In this part we assume for convenience that $n_2 > n_1$. To determine the position parameter b_2 and half width w_2 of EPO-2, we introduce the maximum angle of incidence α_m. From Fig. 3 we see that for an incident ray A_1A_2 with the angle of incidence α_m, the ray is refracted inside the cylinder along ray A_2A_3, then travels inside along ray A_3A_4, and then is refracted out of the cylinder along A_4A_5, which is parallel to the vertical axis. Obviously, a ray with an angle of incidence $\alpha < \alpha_m$ will be refracted out of the cylinder in the backward direction. According to the Snell's law and geometrical relation, the maximum angle of incidence α_m can be calculated using

$$\sin\alpha_m - \frac{n_2}{n_1}\sin\left(\frac{\alpha_m}{2} + \frac{\pi}{8}\right) = 0 \tag{15}$$

Extending A_4A_5 backward until it meets the extension of A_1A_2 at W_2. Thus the line W_2W_2' is the EPO-2 with width of $2w_2$. From Fig. 3, the length of A_2A_0 can be easily found from the ΔOA_2A_0

$$A_2A_0 = a\cos\alpha_m.$$

Fig. 3 Geometry for calculating the position b_2 and the half width w_2 of EPO-2

In ΔOA_2A_4, the angle $\angle OA_2A_4 = 2\beta_m - \pi/2$, and A_2A_4 is given by

$$A_2A_4 = 2a\sin(2\beta_m),$$

where β_m is given by Snell's law $n_1\sin\beta_m = n_2\sin\alpha_m$. In $\Delta A_2A_2'A_4$, there is a relation $\angle A_2'A_2A_4 = 2\beta_m - \alpha_m$, then

$$A_2'A_4 = 2a\sin(2\beta_m)\sin(2\beta_m - \alpha_m).$$

Therefore, the position of EPO-2 can be obtained using the relation $b_2 = A_2'A_4 - A_2A_0$, i.e.

$$b_2 = 2a\sin(2\beta_m)\sin(2\beta_m - \alpha_m) - a\cos\alpha_m. \tag{16}$$

The half size of EPO-2 can be given by

$$w_2 = a\sin\alpha_m. \tag{17}$$

To determine $x'(\alpha)$ for EPO-2, we may consider an incident ray SA with the angle of incidence α refracted into the cylinder with the angle of refraction β as indicated in Fig. 4. The refracted ray propagates in the cylinder along AA_1, which is reflected inside the cylinder along A_1A_2, and then refracted out of the cylinder along A_2P. Extending A_2P backward till it hits EPO-2 at A'. Line up A_2B vertically, which intersects the z-axis at B. From Fig. 4, we have $\gamma_1 = \angle BA_2O = \alpha - 4\beta + \pi/2$, and $\gamma_2 = \angle A_2A'B' = 4\beta - 2\alpha$. In ΔOA_2B,
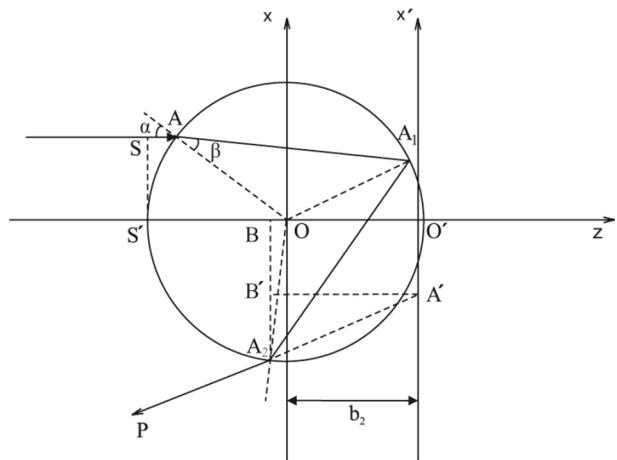
$$OB = a\sin\gamma_1 = a\cos(4\beta - \alpha),$$
$$A_2B = a\cos\gamma_1 = a\sin(4\beta - \alpha).$$

Then $A'B' = b_2 + OB$. In $\Delta A_2A'B'$,

$$A_2B' = A'B'\tan\gamma_2 = \Big(b_2 + a\cos(4\beta - \alpha)\Big)\tan(4\beta - 2\alpha).$$

Thus, for an incident ray SA, the ray refracted out of the cylinder in backward direction can be considered as emitting from point A' at EPO-2 along the line $A'A_2P$. The coordinate of A' can be determined using $x'(\alpha) = A_2B - A_2B'$. We then have

Fig. 4 Geometry for calculating the amplitude $a_2(x')$ and the phase $\phi_2(x')$ of EPO-2

$$x'(\alpha) = a\sin(4\beta - \alpha) - \left(b_2 + a\cos(4\beta - \alpha)\right)\tan(4\beta - 2\alpha). \tag{18}$$

The phase $f_2(x')$ at $A'(x', 0)$ is then given by

$$f_2(x') = k(n_1 SA + n_2 AA_1 + n_2 A_1 A_2 - n_1 A_2 A'), \tag{19}$$

where

$$SA = a(1 - \cos\alpha),$$
$$AA_1 = A_1 A_2 = 2a\cos\beta,$$
$$A_2 A' = \frac{A'B'}{\cos\gamma_2} = \frac{b_2 + a\cos(4\beta - \alpha)}{\cos(4\beta - 2\alpha)}.$$

Taking SS' as the reference line of phase, $\phi_2(x')$ can be given by

$$\phi_2(x') = f_2(x') - kn_1(a + b_2), \tag{20}$$

where $f_2(x')$ is referred to Eq. (19). To determine the amplitude $a_2(x')$, we need to take one reflection and two refractions that the ray undergone into account. Thus we have

$$a_2(x') = exp(-\sigma s)a_2^0(x')|R(x')|T(x'), \tag{21}$$

where

$$a_2^0(x') = \left|\frac{dx}{dx'}\right| = \left|\frac{a\cos\alpha}{dx'(\alpha)/d\alpha}\right|, \tag{22}$$

and the refraction factor $T(x')$ is given by

$$T(x') = t_A(x')t_B(x'). \tag{23}$$

Here σ is the absorption coefficient and s is the distance $s = AA_1 + A_1 A_2$ along the ray inside the cylinder.

For TE wave, the Fresnel reflection and refraction coefficients are given by, respectively,

$$R(x') = \frac{n_2\cos\beta - n_1\cos\alpha}{n_2\cos\beta + n_1\cos\alpha}, \tag{24}$$

$$t_A(x') = \frac{2n_1\cos\alpha}{n_1\cos\alpha + n_2\cos\beta}, \tag{25}$$

$$t_B(x') = \frac{2n_2\cos\beta}{n_1\cos\alpha + n_2\cos\beta}. \tag{26}$$

3 Numerical simulation and discussions

We now apply the formulated CMRD method to the forward modeling and numerical computations for ultra-wideband pulse propagation and backscattering from a perfectly conducting 2-D circular cylinder. In the study of target identification and image processing, a

2-D circular cylinder can be used to model various targets, such as human being or some kind of building structure. Therefore, the investigation on the scattering off the 2-D circular cylinder can not only help understand the physical mechanisms of the interaction between the signal and the target but also is important to the target identification.

Though UWB radar is becoming an appealing technology for detecting and locating the target within the opaque structures, there is still a need for researchers to investigate and develop new models and computation algorithms of UWB signal propagation, especially for the backward propagation and backscattering computation. A deterministic method based on the geometric theory of diffraction (GTD) has been used for modeling and computing UWB signal propagation [12, 13]. Note that the theory for GTD approach is basically much different from that of CMRD. The finite-difference time-domain (FDTD) approach is considered as useful tool for the computation of UWB backscattering [14, 15]. Since the computing algorithm based on FDTD method needs sufficient time and enough space cells to get relatively accurate solutions, such a method significantly increases the computing load that may bring limitations in practice. Therefore, our approach based on CMRD may provide an accurate and efficient method for the computation of UWB backscattering.

3.1 Description of the input UWB pulse

For a general UWB signal propagation, the signal sent by the transmitter can be described as a Gaussian monocycle that is mathematically similar to the first derivative of a Gaussian pulse, i.e.

$$p(t) = \frac{2E_0 t}{\tau^2} \exp\left[-\left(\frac{t}{\tau}\right)^2\right], \tag{27}$$

where the pulse is centered at $t = 0$, the constant E_0 determines the peak amplitude, and τ is the pulse width parameter. Taking the Fourier transform of the Gaussian monocycle, we have

$$P(\omega) = \sqrt{\pi} E_0 \tau \omega \exp\left[-\frac{\tau^2}{4}\omega^2\right], \tag{28}$$

where $\omega = 2\pi f$, and f is signal frequency. The Gaussian monocycle pulse shape in time domain and its magnitude spectrum are plotted in Figs. 5a, b. Note that the maximum magnitudes of the monopulse and spectrum are normalized to unity and 0 dB, respectively.

3.2 Backscattering from a 2-D Circular Cylinder Behind a Wall

We now consider a plane wave of UWB pulse is incident on the target of a perfectly conducting 2-D circular cylinder through a wall, as shown in Fig. 6. According to the electromagnetic theory and the CMRD theory discussed above, for a scatterer being a perfectly conducting 2-D circular cylinder, there will be no contribution from EPO-2. If the wall is removed, it becomes a free-space problem. For the backward-scattered signal from a 2-D circular cylinder calculated or measured in frequency domain, the inverse Fourier transform can be employed to obtain the data in time domain. Therefore, we can computed the backward-scattered signals using Eq. (9) together with Eqs. (10), (12),
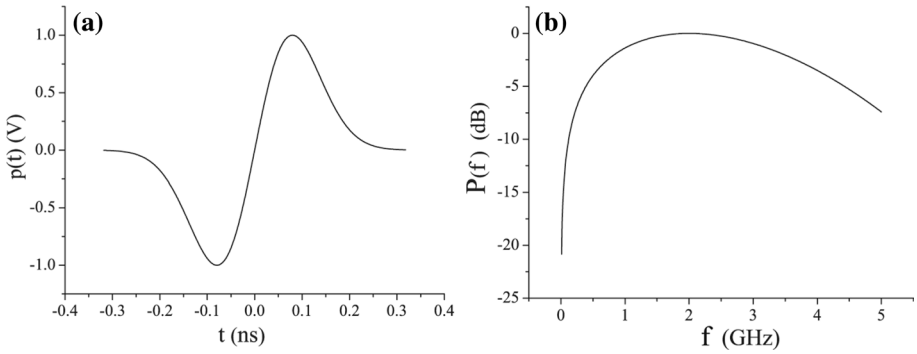
Fig. 5 Gaussian monocycle pulse shape in time domain and its Fourier transform. **a** Pulse waveform of Gaussian monocycle. **b** Frequency spectrum of Gaussian monocycle
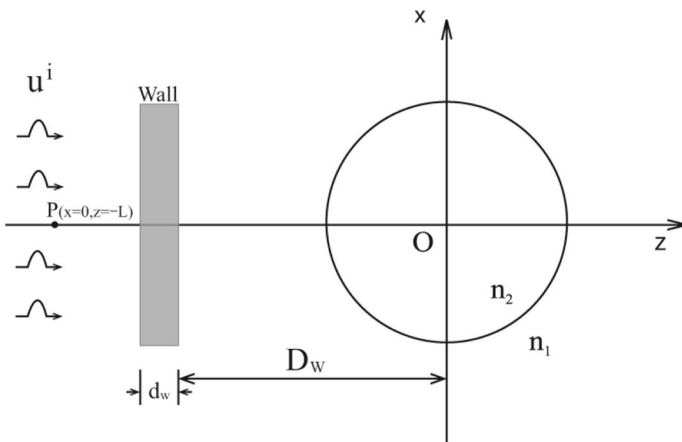

Fig. 6 Diagram of the backscattering of UWB pulse from a 2-D circular cylinder behind a wall

(13), and (14). In addition, the complex reflection coefficient $R_1(x')$ used in Eq. (13) for TM and TE wave has the following forms, respectively,

$$R_1^{TM}(x') = \frac{\cos \alpha_i - \sqrt{\frac{\hat{\epsilon}_2}{\epsilon_1} - \sin^2 \alpha_i}}{\cos \alpha_i + \sqrt{\frac{\hat{\epsilon}_2}{\epsilon_1} - \sin^2 \alpha_i}}, \tag{29}$$

and

$$R_1^{TE}(x') = \frac{-\cos \alpha_i + \sqrt{\frac{\epsilon_1}{\hat{\epsilon}_2}} \sqrt{1 - \left(\frac{\epsilon_1}{\hat{\epsilon}_2}\right) \sin^2 \alpha_i}}{\cos \alpha_i + \sqrt{\frac{\epsilon_1}{\hat{\epsilon}_2}} \sqrt{1 - \left(\frac{\epsilon_1}{\hat{\epsilon}_2}\right) \sin^2 \alpha_i}}, \tag{30}$$

where α_i is the local incident angle, and ϵ_1 and ϵ_2 are the dielectric constants of the surrounding medium (air) and the conducting cylinder, respectively.

When a homogeneous, single-layered wall exists between the signal transmitter and the target as indicated in Fig. 6, the UWB signal propagating through the wall will simply be calculated using geometrical optics. Based on Eq. (9), we have

$$u^{BS}(x,z,f) = \frac{1}{\sqrt{i\lambda_1}} t_{w1}^2 t_{w2}^2 \exp(-2ik_w d_w) \int_{-w_1}^{w_1} [a(x')e^{i\phi(x')} - 1] \frac{z}{R^{3/2}} e^{ik_1(R+s_x^i x'+s_z^i b)} dx',$$

(31)

where f is the UWB signal frequency indicated in Fig. 5b, k_w and d_w are the wavenumber and thickness of the wall, $\exp(-2ik_w d_w)$ is the phase delay factor. t_{w1} and t_{w2} are the transmission coefficients for the UWB signal normally incident on the wall, i.e.

$$t_{w1} = \frac{2n_1}{n_1 + n_w}, \quad t_{w2} = \frac{2n_w}{n_1 + n_w},$$

where n_w is the refractive index of the wall.

3.3 Numerical Results and Discussions

The first purpose of the numerical calculations carried out in this section is to valid the CMRD-based computation method developed in this paper. For this purpose, the backscattering of UWB pulse from a 2D perfectly conducting circular cylinder in free space is computed using the developed method, which is compared to that obtained from the exact eigenfunction expansion method for an impulsive TE and TM plane wave with unit amplitude, respectively. The second purpose comes from the intention of imaging processing and target identification using backscattering measurements of UWB signals, which leads to that we carry out the computations of the backscattering of UWB pulse from a 2D perfectly conducting circular cylinder behind different walls together with comparisons and discussions.

3.3.1 Numerical Results for the Cylinder in Free Space

The incident pulse is a Gaussian monocycle. The values of other parameters are assumed to be as follows: the peak amplitude of the pulse equals unity, frequency bandwidth of the pulse is $f = 1.0-3.5$ GHz, and the refractive index of the surrounding medium (air) is $n_1 = 1$. Note that the observation point P is at $(x, z) = (0, -L)$ and the radius of the circular cylinder a will be varied for different computations. The scattered signal from a perfectly conducting 2-D circular cylinder is calculated using Eq. (31), for an impulsive TE or TM plane wave with unit amplitude, while the same case calculation is also carried out using the eigenfunction expansion method [6]. The numerical results and comparisons are shown in Figs. 7a–d.

Figures 7a–d show that good agreements are achieved. It also indicates that there is a better achieved agreement for the cases that the radius of the cylinder a is smaller (see Figs. 7a, c), which can be predicted with the following explanations. It is well known that eigenfunction expansion method gives useful and accurate results only if ka is not too large compared to unity [6], while Kirchhoff diffraction theory results in more and more accurate solutions if $ka \geq 1$ [10].
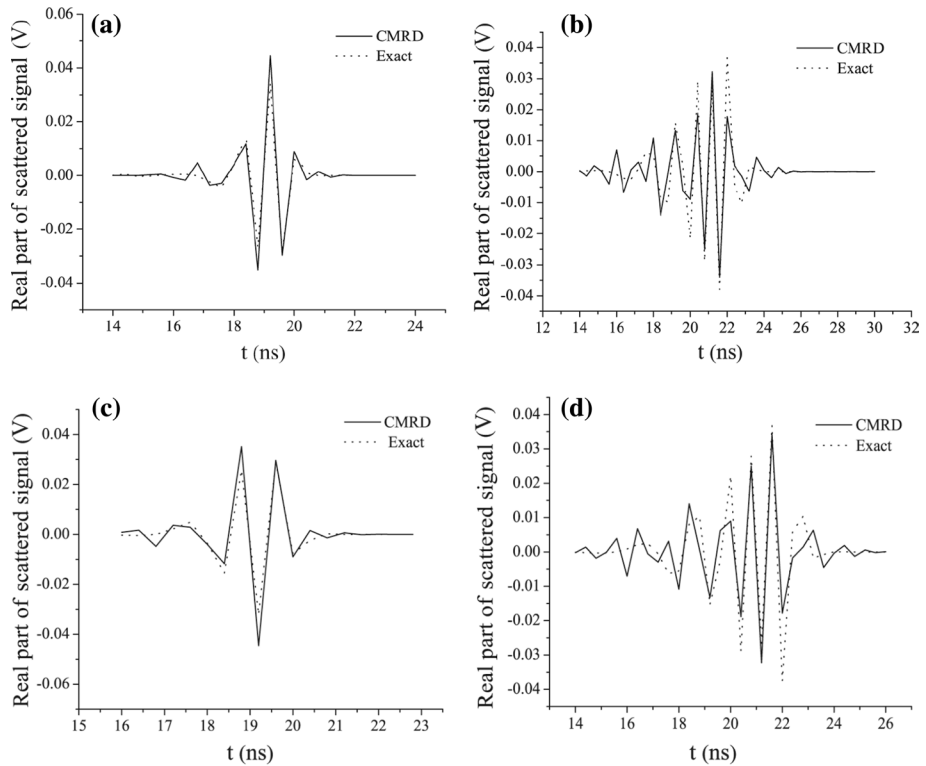
Fig. 7 Comparison of the backscattered signals from a perfectly conducting circular cylinder in free space: **a** $L = 10$ m, $a = 0.2$ m, TE polarized. **b** $L = 10$ m, $a = 0.5$ m, TE polarized. **c** $L = 10$ m, $a = 0.2$ m, TM polarized. **d** $L = 10$ m, $a = 0.5$ m, TM polarized

3.3.2 Numerical Results for the Cylinder Behind a Wall

We now put a homogeneous, single-layered wall with thickness of d_w in front of the 2-D perfectly conducting circular cylinder as shown in Fig 6, and the position of the wall is $z = -D_w$. The observation point P is at $(x, z) = (0, -L)$. The input signal is a TM polarized Gaussian monocycle. Figures 8a, b present the plots of calculated backward-scattered signals from the cylinder for brick and adobe walls with different dielectric constants.

Time delay can be seen from the results of Figs. 8a, b. From the computed numerical values of Fig. 8, the time difference in time delay between the brick and adobe walls is $\delta t = 0.016$ ns. We can also use $\delta t = 2d_w/v$ to compute the time difference in time delay between the brick and adobe walls, which yields a result that $\delta t = 0.014$ ns. From this comparison, we can conclude that the results of numerical simulation give a good evaluation of the time delay, which may be important for the design of the signal receiver. Beside the time delay, we also see from Fig. 8 that the curve shape and the amplitude of curve are quite different, which cannot be explained using geometrical optics. The signal obtained at $P(x, z)$ basically represents the diffraction of the equivalent phase object of the perfectly conducting circular cylinder, as a function of few physical parameters, which shows the possibility of that the developed CMRD method above can be used to
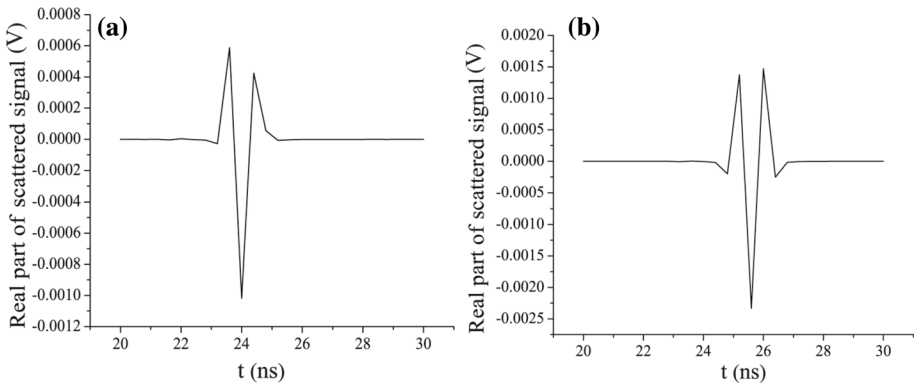
Fig. 8 The backscattered signal from a 2-D circular cylinder behind the wall in time domain with $d_w = 0.3$ m, $D_w = 2.5$ m, $L = 10$ m, and $a = 0.2$ m. **a** Brick wall; **b** adobe wall

retrieve the physical parameters, such as the refractive index, radius, and location of the cylinder, dielectric constant of the wall, and so on.

The numerical results of $P(x, z)$ indicated in Figs. 7 and 8 are obtained efficiently and accurately using the developed computation algorithm based on CMRD method. Note that the computation or measurement of $P(x, z)$ can be done for the positions of $x \neq 0$.

4 Conclusions

We have presented theoretical analyses, formulated discussions, and numerical computations for the backscattering computation using the combined method of ray tracing and diffraction (CMRD). Especially, the concept of the equivalent phase object (EPO) is emphasized and considered as the most important part in the developed CMRD method, which is explained mathematically with accurately derived expressions for the amplitude and the phase functions of the EPO. Numerical simulations are carried out with applying the formulated CMRD method to the forward modeling and backscattering computations for ultra-wideband pulse propagation and backscattering from a perfectly conducting 2-D circular cylinder. From numerical results, we can conclude that there are good agreements achieved with comparisons between our CMRD method and exact eigenfunction expansion approach. Numerical curves basically represent the diffraction of the equivalent phase object of the perfectly conducting circular cylinder, which shows the possibility of that the developed CMRD method in this study can be used to retrieve the physical parameters of the observed cylinder and background. It is expected that the theoretical model and method of backscattering calculation using CMRD can be applied to the image processing and target identification with backscattered measurements of electromagnetic and acoustic waves.

References

1. Ruppin, R. (1990). Electromagnetic scattering from finite dielectric cylinders. *Journal of Physics D: Applied Physics*, *23*, 757–763.
2. Houdzoumis, V. A., Wu, T. T., & Myers, J. M. (1996). Backscattering of an electromagnetic missile by a metal cylinder of degree higher than two. *Journal of Physics*, *80*, 15–24.
3. Zhu, D., & Bjorno, L. (2000). A three-dimensional, two-way, parabolic equation model for acoustic backscattering in a cylindrical coordinate system. *Journal of the Acoustical Society of America*, *108*(3), 889–898.
4. Jech, J. M., Horne, J. K., Chu, D., Demer, D. A., Francis, D. T. I., Gorska, N., et al. (2015). Comparisons among ten models of acoustic backscattering used in aquatic ecosystem research. *Journal of the Acoustical Society of America*, *138*(6), 3742–3764.
5. Shang, Y., Shen, Z., & Feng, K. (2016). Enhancement of backscattering by a conducting cylinder coated with gradient metasurface. *Journal of Applied Physics*, *120*, 045109.
6. Bowman, J. J., Senior, T. B. A., & Uslenghi, P. L. E. (1969). *Electromagnetic and acoustic scattering by simple shapes*. Amsterdam: North-Holland Publishing Company.
7. Mitri, F. G. (2010). Acoustic backscattering enhancements resulting from the interaction of an obliquely incident plane wave with an infinite cylinder. *Ultrasonics*, *50*, 675–682.
8. La Follett, J. R., Williams, K. L., & Marston, P. L. (2011). Boundary effects on backscattering by a solid aluminum cylinder: Experiment and finite element model comparisons (L). *Journal of the Acoustical Society of America*, *130*(2), 669–672.
9. Chen, B., & Stamnes, J. J. (1998). Scattering by simple and nonsimple shapes by the combined method of ray tracing and diffraction: Application to circular cylinders. *Applied Optics*, *37*(11), 1999–2010.
10. Stamnes, J. J. (1986). *Waves in focal regions*. Bristol: Hilger.
11. Stamnes, J. J., Spjelkavik, B., & Pedersen, H. M. (1983). Evaluation of diffraction integrals using local phase and amplitude approximations. *Optica Acta*, *30*, 207–222.
12. Potter, L. C., & Moses, R. L. (1997). Attributed scattering centers for SAR ATR. *IEEE Transactions on Image Processing*, *6*(1), 79–91.
13. Qiu, R. C. (2004). A generalized time domain multipath channel and its application in ultra-wideband (UWB) wireless optimal receiver design—Part II: Physics-based system analysis. *IEEE Transactions on Wireless Communications*, *3*(6), 2312–2324.
14. Zhao, Y., Hao, Y., & Parini, C. (2007). FDTD characterization of UWB indoor radio channel including frequency dependent antenna directivities. *IEEE Antennas and Wireless Propagation Letters*, *6*(11), 191–194.
15. Christodoulou, C., Railton, C. J., Klemm, M., Gibbins, D., & Craddock, I. J. (2012). Analysis of a UWB emispherical antenna array in FDTD with a time domain Huygens method. *IEEE Transactions on Antennas and Propagation*, *60*(11), 5251–5258.

Bingquan Chen was born in China in 1963. He received the B.S. degree in applied physics from Dalian University of Technology (Dalian, China, 1986), the M.S. degree in applied physics from National Institute of Metrology (Beijing, China, 1991), and the Ph.D. degree in optics from University of Bergen (Bergen, Norway, 1996). He is currently a professor with School of Sciences, Qingdao University of Technology. His research interests mainly include quantum theory, EM wave propagation, and related fields.

Chang Chen was born in China in 1979. He received the B.S. degree in applied physics from Yunnan University (Kunming, China, 2001), the M.S. degree in particle physics from Yunnan University. He is currently a lecturer with School of Sciences, Qingdao University of Technology. His research interests mainly include experimental physics and optical imaging.

Hongyang Ma was born in China in 1976. He received the B.S. degree in applied electronics technology from Qufu Normal University, Shandong, China, in 1994, and the M.S. and Ph.D. degrees in computer science and technology from Ocean University of China, Qingdao, China. He is currently a professor with School of Sciences, Qingdao University of Technology. His research interests mainly include quantum network, wireless network, information security theory, and related fields.